Tuijin Jishu/Journal of Propulsion Technology
ISSN: 1001-4055
Vol. 44 No. 3 (2023)

Effect of Chemical reaction on hyperbolic tangent Williamson-Nanofluid flow past an exponentially porous stretching sheet: MHD and slip effects

[1*]R. S. DurgaRao, [2]R. Vijayakumar, [3]V. Vasudeva Murthy

[1] Department of Mathematics, Vishnu Institute of Technology, Bhimavaram,West Godavari (Dt), 534202,
Andhra Pradesh, India.
[2] Department of Mathematics, Periyar Government Arts College, Cuddalore, 607001, Tamilnadu State, India.
[3] Department of Mathematics, S. R. K. R. Engineering College, Bhimavaram, West Godavari (Dt), 534202,
Andhra Pradesh, India.

*Corresponding author Email address: rathirath_viji@yahoo.co.in

Abstract: In this research investigation, Runge-Kutta method solutions of dual-dimensional, steady, viscous, incompressible, chemically reacting, electrically conducting, hyperbolic tangent Williamson- flow of nanofluid past a uni-directional an while a magnetic field is present and several slip effects, an exponentially stretched sheet packed with porous material is studied numerically. Thermal radiation, Chemical reaction, the flow regulatingequations of boundary layer incorporates the impacts of thermophoresis and Brownian motion.SuitableTransformations of similarity are employed. for the main differential equations in partial to become differential equations inordinary that are nonlinear. The resultant governing equations are resolved by the application of a well utilized method in numericallycalled as the Runge-Kutta method and the shooting technique.Figures and numerical tables are used to show the representation of certain physical parameters on the flow model.. The pace of convergence for nonlinear differential systems is astonishing, according to an excellent comparison with the body of existing research, which also confirms a high degree of correctness. These tests are pertinent to the fields of plastic films, crystal growth, paper manufacture, and metal sheet cooling.
Keywords: Hyperbolic tangent Nanofluid; Williamson fluid; Magnetic field; Nanofluid; Chemical reaction; Thermal radiation; Porous medium;Exponentially Stretching sheet; Runge-Kutta method;

Nomenclature

Symbols List:

u, v : In x and y axes velocity components, accordingly (m/s)

x, y : Coordinates along the stretched sheetCalculated Cartesian (m)

f : Stream function without dimensions

f' : Fluid'Velocity(*m*/*s*)

Pr : Prandtl number

T : Temperature of the Fluid(*K*)

C : fluid's volume concentration nanoparticles (mol / m^3)

T_w : Surface Temperature (*K*)

C_∞ : Dimensional ambient fraction of volume (mol / m^3)

C_w : Concentration of dimensional nanoparticles near the stretching surface (mol / m^3)

B_o : Consistent magnetic field (*Tesla*)

M : Parameter of Magnetic field

T_∞ : The fluid's temperature at a length from the stretched sheet (*K*)

Cf : **C**oefficient ofSkin-friction (s^{-1})

Nb : Brownian motion 's Parameter

u_w : stretching velocity of the Fluid(*m*/*s*)

Nu : Heat transfer rateCoefficient (or) Nusselt number

Nt : Parameter ofThermophoresis

Sc : Schmidt digit

q_w : Coefficientof Heat flux

q_m : Mass flux Coefficient

C_p : The nanoparticles' particular heat capacity ($J / kg / K$)

D_B : Coefficient of Brownian diffusion

D_T : Diffusion of thermophoresiscoefficient (m^2 / s)

Sh : Sherwood number

K : PermeabilityParameter (m^{-1})

k_1 : Porous mediumPermeability (m^{-1})

Re_x : Reynold's number

S : Suction/Injection parameter

R : Parameter of Thermal radiation

q_r : Heat flux radiative

K^* : Mean absorption's Coefficient

n : Power-law index parameter

$B(x)$: Magnetic field function (*Tesla*)

O : Origin

U_w : velocity reference (m/s)

V_o : Mass transfer velocity (m/s)

L_1 : ThermalSlip length(m)

L_2 : Concentration slip length (m)

L : Length of slip (m)

Kr : Chemical reaction parameter with dimensions

Greek symbols

η :Dimensionless similarity Variable (m)

θ :Temperature that is indimensional less(K)

ϕ :Concentration of non-dimensional nanoparticles (mol / m^3)

α : The diffusivity of heat, (m^2 / s)

ν : Motion Viscosity (m^2 / s)

σ : Conductivity of electricity

ρ : Density ofFluid, (kg / m^3)

μ : Fluid's Dynamic viscosity

κ : Fluid'sThermal conductivity, ($W / (m \cdot K)$)

τ_w : Shear stress

δ : Heat slip coefficient

Δ : Concentration slip coefficient

β : Non-dimensional parameter for chemical reaction

λ : Parameter Williamson fluid

σ^* : Stefan Boltzmann constant

ϑ : Stretching sheet parameter

Γ : Shear stress (s^{-1})

τ_B : Cauchy Stress tensor

Superscript:

$'$: Differentiation w.r.t η

Subscripts:

f : Fluid,

w : status on the sheet,

∞ : Ambient Conditions.

1. Introduction:

Non-Newtonian fluid analysis has increase in significance in current studies because Newtonian fluid applications are limited. Non-Newtonians in fluids in everyday life added, flour, honey, hydraulic fluids, and lubricating sprays. Shear stress does not inversely correspond in non-Netonian fluids with shear rate. Shear thickening fluids and shear thinning fluids are the two categories of non-Newtonian fluids.Chemistry frequently deal with non-Newtonian fluids mechanics, and biology. It has caught the interest of many scholars interested in blood, lubrication, and plasma flow. Several fluid models built to simulate the properties of actual fluids at different viscosities. These fluid models can help you better grasp rheological characteristics of fluids that are not Newtonian. Examples include the liquids Jaffrey, Maxwell, Casson, Williamson, Carreau, and others. There was no appropriate mathematical model that adhered to pseudoplastic (shear thinning) fluid flow. By investigating pseudoplastic materials and creating the non-Newtonian fluid model that bears his name, Williamson [1] pioneered the field. The first appearance of this model occurred in 1929. Due to its popularity, several studies (Kumar et al. [2] and Ahmed et al. [3] have used this model in order to illustrate the actual action of fluids during the past ten years.By taking temperature and velocity into account, Lund et al. [4] confirmed the

MHD Williamson fluid flow on a stretched sheet.Kumar et al. [5] looked into the consequences of MHD Williamson fluid flow with a changeable heat sink or source over a flat or curved surface that is chemically reactive. Megahed [6] examined fluid of Williamson created by a surface in motion while accounting for viscous dissipation. Wall shear parameters were taken into account in Gireesha et al.'s [7] analysis of Williamson fluid movement within a little channel. Bhatti et al.'s [8] A detailed analysis of the effects of entropy creation for a Williamson fluid in MHD made use of a wedge's surface permeability. In manufacturing and engineering. Dawar et al. [9] looked at heat exchanger issues, the importance of flexibility, and boundary layer fluid flows. According to Li et al. [10], MHD has uses in a number of industries, such as agriculture, petroleum, and medical. Patil et al. [11] investigated how radiation affected the Williamson nanofluid's permeable, stretched sheet movement using MHD.NanofluidWilliamson wasverified by Awan et al. [12] inside a sheet-stretching geometry to determine how radiation in nonlinearilyand exponential heat sources affected it.Over an exponentially stretched porous curved surface, a mixed convection flow with magnetohydrodynamic (MHD) properties contains a Williamson-type fluid. Ahmed et al. [13] assess the mechanism of heat transfer. Generalized non-Fourier models developed by Nazir et al. [14] are employed in Williamson fluid to investigate transport via mass and heat.Their research on the stratified electro-magneto hydrodynamic flow of nanofluid, Yahaya Shagaiya Daniel et al. explored the special properties of twofold division([15]-[17]). High performance and energy efficiency are made possible by this architecture without the need of additional electricity. Fazle Mabood et al. [18] examined radiation's impact on a heated MHD surface's Williamson nanofluid. The mathematical model for the creation of the Williamson nanofluid on a radially expanded surface by Webshet Ibrahim and DachasaGamachu [19]. The radiative Williamson nanofluid MHD Blasius floweffects on a slanted plate were quantitatively verified by Aamir Hamid et al. [20]. Similar numerical methods were developed by Shawky et al. [21] across a in a porous mediafor verification the Defour-Sorét effect of the nanofluid of Williamson, a stretched sheet. The relationship between thermal radiation and the slip flow of the Williamson approach was determined by Prasannakumar et al. [22] using the Runge-KuttaFelhbergorder and a firing mechanism. Hunenberg [23] created a computer solution for an unstableflow through a stretched, heated, permeable sheet with viscous dissipation utilizing the shooting method and the R-K fourth order. Williamson nanofluid MHD flow was investigated by Tanvir Akbar and Kamran Ahmed [24] on a surface that is stretched exponentially. Hashim et al. [25] verified the Mechanisms transmission of heat and mass of moving nanoparticles in Williamson fluids.

According to the literature review, the joint impacts Brownian motion and thermophoresis on a two-dimensional, stable, viscous, and incompressible chemically reacting, electrically conducting, hyperbolic tangent Nanofluid Williamson flow over a unidirectional, Multiple slip effects and an exponentially stretched sheet using a magnetic field present and packed with porous material are clearly examined numerically. Plotting graphs for various Williamson parameters allows one to see the way non-newtonian fluids behave. Additionally, The physical quantities that were of specific importance were totaled. Plotting graphs for various Williamson parameters allows one to see the behaviour of non-Newtonian fluids. In additionparticular physical quantities of relevance were totalled. We hope that our work will help to clarify and explore the mechanics of stretching in exponential geometry within a more practical context.

2. Governing Equations for Flow

In this research, he combined effects of a magnetic field and porous material on Brownian motion and thermophoresis on a steady two-dimensional flow of Williamson-nano fluid approaching a non-linearly stretched sheet. The physical coordinate and problem geometry is shown in Fig. 1. The following presumptions are taken into account for this study.

i. The boundary-layer occurs at $y \geq 0$, when the coordinate is assigned the stretching surface's normal.
ii. The Williamson-nano fluid flow, which is convective and stable, has a boundary layer when a Consistent magnetic field of strength B_o is present.
iii. The current approach uses thermophoresis and Brownian motion to describe the movement of the nanoparticles in the base fluid.

iv. From the wall on the boundaries the nanoparticle temperature andvolume concentration C are believed to be T_w and C_w, at the wall, T_∞ and C_∞, individually are distant.

v. The sheet is thought to contract exponentially with velocity $u_w(x) = U_w e^{\frac{x}{L}}$, (1)

vi. Additionally, in the magnetic field B (x) is thought to be of the following form $B = B_o e^{\frac{x}{L}}$, (2)

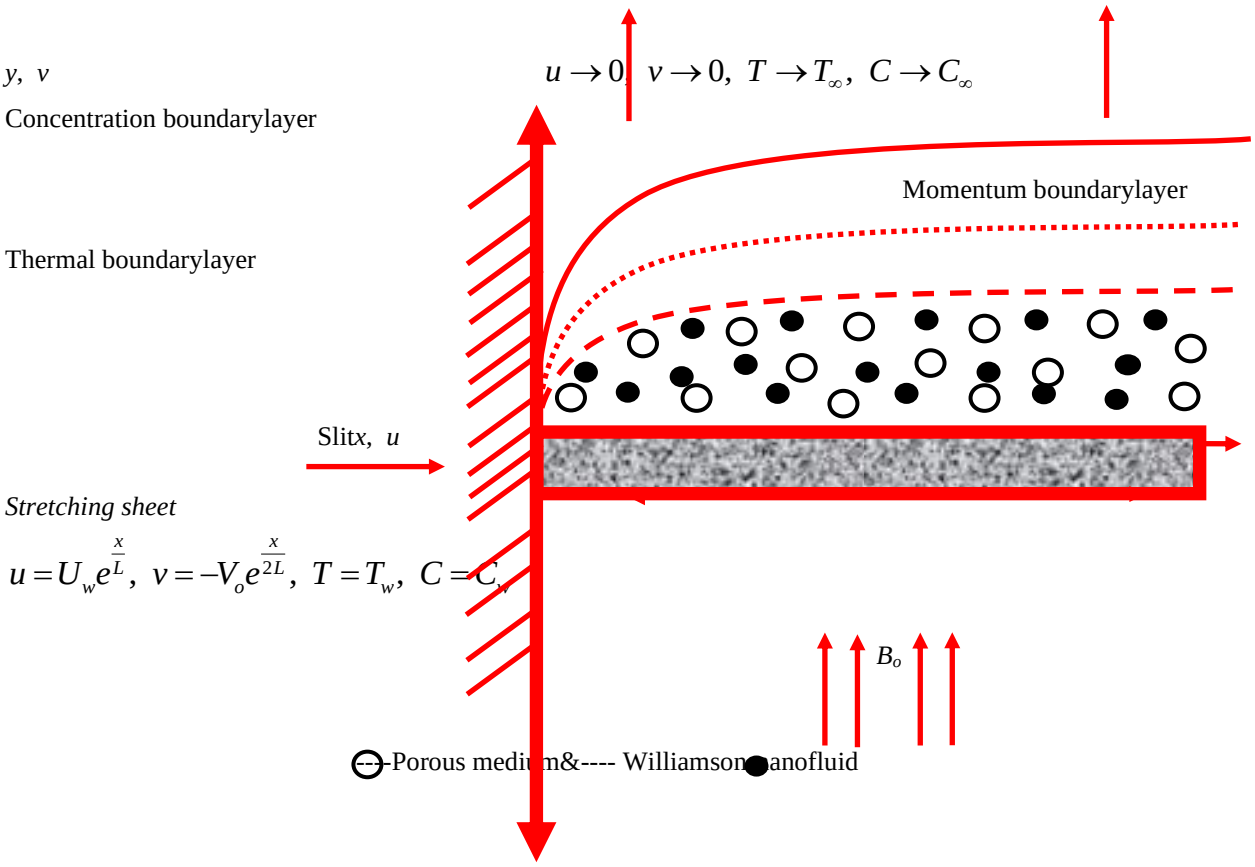

Fig 1: Williamson-nanofluid shape shown geometrically

On the basis of the aforementioned the two-dimensional, electrically conducting, incompressible boundary layer equations, and stable presumptions, hyperbolic tangent Williamson-nano fluid flow are:

Continuity Equation:

$$\left[\frac{\partial u}{\partial x}\right] + \left[\frac{\partial v}{\partial y}\right] = 0, \quad (3)$$

Momentum Equation:

$$u\left[\frac{\partial u}{\partial x}\right] + v\left[\frac{\partial u}{\partial y}\right] = \nu(1-n)\left[\frac{\partial^2 u}{\partial y^2}\right] + \sqrt{2}\nu n\Gamma\left[\frac{\partial u}{\partial y}\right]\left[\frac{\partial^2 u}{\partial y^2}\right] - \nu\left[\frac{u}{k_1}\right] - \left[\frac{\sigma B_o^2}{\rho}\right]u, \quad (4)$$

Thermal energy Equation:

$$u\left[\frac{\partial T}{\partial x}\right]+v\left[\frac{\partial T}{\partial y}\right]=\alpha\left[\frac{\partial^2 T}{\partial y^2}\right]+\tau_B\left\{D_B\left[\frac{\partial C}{\partial y}\right].\left[\frac{\partial T}{\partial y}\right]+\frac{D_T}{T_\infty}.\left[\frac{\partial T}{\partial y}\right]^2\right\}-\frac{1}{\rho C_p}\left[\frac{\partial q_r}{\partial y}\right], \quad (5)$$

Equation of species nanoparticle volume concentration:

$$u\left[\frac{\partial C}{\partial x}\right]+v\left[\frac{\partial C}{\partial y}\right]=D_B\left[\frac{\partial^2 C}{\partial y^2}\right]+\frac{D_T}{T_\infty}\left[\frac{\partial^2 T}{\partial y^2}\right]-Kr\left(C-C_\infty\right), \quad (6)$$

The flow's boundary conditions are

$$\left.\begin{array}{l} u=u_w\left(x\right)=U_w\,\mathrm{e}^{\frac{x}{L}},\ v=v_w\left(x\right)=V_o\,\mathrm{e}^{\frac{x}{2L}},\ T=T_w+L_1\left(\frac{\partial T}{\partial y}\right),\ C=C_w+L_2\left(\frac{\partial C}{\partial y}\right)\ at\ \ y=0 \\ u\to 0,\ v\to 0,\ T\to T_\infty,\ C\to C_\infty\ \ as\ \ y\to\infty \end{array}\right\}, \quad (7)$$

The heat flow radiative q_r is defined (using Rosseland approximation) as

$$q_r=-\frac{4\sigma^*}{3K^*}\left(\frac{\partial T^4}{\partial y}\right) \quad (8)$$

We make the assumption that the term T^4 because of the temperature fluctuations inside the flow, may be represented as a temperature as a linear function.The subsequent to get this about a free stream temperature T^4, apply the Taylor series expansion:

$$T^4=T_\infty^4+4T_\infty^3\left(T-T_\infty\right)+6T_\infty^2\left(T-T_\infty\right)^2+\ldots\ldots\ldots \quad (9)$$

Once the first degree term in the above equation has been eliminated, major order terms in $\left(T-T_\infty\right)$, we have

$$T^4\cong 4T_\infty^3T-3T_\infty^4 \quad (10)$$

ThusapplyingEq. (10) in Eq. (8), weget

$$q_r=-\frac{16T_\infty^3\sigma^*}{3K^*}\left(\frac{\partial T}{\partial y}\right) \quad (11)$$

Using (11), Eq. (5) can be written as

$$u\left[\frac{\partial T}{\partial x}\right]+v\left[\frac{\partial T}{\partial y}\right]=\alpha\left[\frac{\partial^2 T}{\partial y^2}\right]+\tau_B\left\{D_B\left[\frac{\partial C}{\partial y}\right]\left[\frac{\partial T}{\partial y}\right]+\frac{D_T}{T_\infty}\left[\frac{\partial T}{\partial y}\right]^2\right\}+\frac{1}{\rho C_p}\left[\frac{16T_\infty^3\sigma^*}{3K^*}\right]\left[\frac{\partial^2 T}{\partial y^2}\right], \quad (12)$$

We introduce the following transformations of similarity

$$u=U_o\,\mathrm{e}^{\frac{x}{L}}\,f'\left(\eta\right),\ v=-\sqrt{\frac{\nu U_o}{2L}}\,\mathrm{e}^{\frac{x}{2L}}\left\{f\left(\eta\right)+\eta f'\left(\eta\right)\right\},\ \eta=y\sqrt{\frac{U_o}{2\nu L}}\,\mathrm{e}^{\frac{x}{2L}},\ \phi=\frac{C-C_\infty}{C_w-C_\infty},\ \theta=\frac{T-T_\infty}{T_w-T_\infty}, \quad (13)$$

Using Eq. (13),The continuity equation is satisfied in the same way. The resulting equations of Eqs(4), (6) and (12) are

$$\left(1-n\right)f'''+ff''+n\lambda f'''\,f''-\left(M+K\right)f'-2\left(f'^2\right)=0, \quad (14)$$

$$\left(1+\frac{4R}{3}\right)\theta''+\beta\,\mathrm{Pr}\,f\theta'+\mathrm{Pr}\,Nb\theta'\phi'+\mathrm{Pr}\,Nt\left(\theta'\right)^2=0, \quad (15)$$

$$Nb\phi''+ScNbf\,\phi'+Nt\theta''-\beta Nb\phi=0, \quad (16)$$

The corresponding boundary conditions (6) shift to

$$\left.\begin{array}{l} f(0)=S,\ f'(0)=\vartheta,\ \theta(0)=1+\delta\theta'(0),\ \phi(0)=1+\Delta\phi'(0) \\ f'(\infty)\to 0,\ \theta(\infty)\to 0,\ \phi(\infty)\to 0 \end{array}\right\}, \quad (17)$$

the physical characteristics involved are described as

$$\left.\begin{array}{l} M=\dfrac{2\sigma B_o^2 L}{\rho U_o}e^{\frac{-x}{L}},\ \vartheta=\dfrac{U_w}{U_o},\ \mathrm{Pr}=\dfrac{\nu}{\alpha},\ Nb=\dfrac{(\rho C)_p.D_B.(C_w-C_\infty)}{\nu(\rho C)_f}e^{\frac{x}{2L}}\sqrt{\dfrac{U_o}{2\nu L}}, \\ S=V_o\sqrt{\dfrac{2L}{\nu U_o}},\ \beta=\sqrt{\dfrac{U_o}{2\nu L}}e^{\frac{x}{2L}},\ Nt=\dfrac{(\rho C)_p.D_T.(T_w-T_\infty)}{\nu T_\infty(\rho C)_f}e^{\frac{x}{2L}}\sqrt{\dfrac{U_o}{2\nu L}},\ Sc=\dfrac{\nu}{D_B}, \\ \lambda=\Gamma\sqrt{\dfrac{U_o^3 e^{\frac{3x}{L}}}{\nu L}},\ K=\dfrac{2\nu L}{k_1 U_o}e^{-\frac{x}{L}},\ R=\dfrac{4T_\infty^2\sigma^*}{\kappa^*\alpha\rho C_p},\ \delta=L_1\sqrt{\dfrac{U_o}{2\nu L}}e^{\frac{x}{2L}},\ \Delta=L_2\sqrt{\dfrac{U_o}{2\nu L}}e^{\frac{x}{2L}}, \end{array}\right\}, \quad (18)$$

The local Sherwood number, Nusselt number, coefficient of skin-friction, and quantities of physical relevance are displayed here:

$$C_f=\left\{\frac{\tau_w}{\rho U_w^2}\right\}_{y=0}=\left[\frac{1}{\rho U_w^2}\left\{(1-n)\left(\frac{\partial u}{\partial y}\right)+n\left(\frac{\Gamma}{\sqrt{2}}\right)\left(\frac{\partial u}{\partial y}\right)^2\right\}\right]_{y=0} \quad (19)$$

$$\Rightarrow Cf=\left(\sqrt{\mathrm{Re}_x}\right)C_f=\left[(1-n)+\frac{n\lambda}{2}f''(0)\right]f''(0)$$

$$Nu=\frac{Lq_w}{\kappa(T_w-T_\infty)}=-\frac{L\kappa\left(\frac{\partial T}{\partial y}+\frac{\partial q_r}{\partial y}\right)_{y=0}}{(T_w-T_\infty)}\Rightarrow Nu=-\left(1+\frac{4R}{3}\right)\left(\sqrt{\frac{\mathrm{Re}_x}{2}}\right)\theta'(0)$$

(20)

$$Sh=\frac{xq_m}{D_B(T_w-T_\infty)}\ \text{where}\ q_m=-D_B\left(\frac{\partial C}{\partial y}\right)_{y=0}\Rightarrow \mathrm{Re}_x^{-\frac{1}{2}}Sh=-\phi'(0) \quad (21)$$

Where $\mathrm{Re}_x=\dfrac{U_o x\left\{\exp\left(\frac{x}{L}\right)\right\}}{\nu}$ be the local Reynolds number.

3. Solution Method by Runge-Kutta method:

An accurate solution for the whole set of equations (14)–(16) does not appear to be achievable. This is because (14)–(16) are non-linear, and Eq. (17) provides appropriate boundary conditions. Therefore, Numerical techniques are necessary to resolve the problem. The controlling Using similarity transformations, set of numerically solvable non-linear ordinary differential equations is produced from a set of partial differential equations.Using the shooting strategy in conjunction with a fourth-order Runge-Kutta scheme, the resultant boundary value problem is numerically solved. The nonlinear differential equations may be reduced to a collection of differential equations of order one. Obtainedone set of differential equations of first order. Seven simultaneous equations for seven unknowns in the system represents the simplified form of the coupled ordinary differential equations (14) – (16), as seen in the figure.Third order coupled ordinary differential equations (14)–(16). $f(\eta)$ and in $\theta(\eta)$ and $\phi(\eta)$ in secondorder which are now only seven simultaneous equations with seven unknowns. Seven prerequisites must be completed in order to use the Runge-Kutta technique to numerically

solve this system of equations,but in $f(\eta)$two initial conditions,primaryinitial condition in eachof $\theta(\eta)$ and $\phi(\eta)$ are recognized. However, the values of $f'(\eta)$,$\theta(\eta)$ and $\phi(\eta)$ are known at $\eta \to \infty$. usingshooting techniquethese last conditions are used to generate starting conditions that are unknown at $\eta = 0$. The most crucial part of this plan is determining the suitable limited value ofη_∞. In order to determine the value of η_∞beginning with a preliminary estimate, we address the boundary value issue using Equations. (14)-(16) toobtain $f''(0), \theta'(0)$ and $\phi'(0)$. in addition to a greater value of $\eta_\infty$the solution process is repeateduntil two consecutive valuesof $f''(0)$, $\theta'(0)$ and $\phi'(0)$ variate afteronly desired significantdigit. The final value η_∞ is consider as thelast value of the limit$\eta_\infty$for the specific collection of physical characteristics used to calculate concentration, temperature, and velocity, respectively, are $f(\eta)$, $\theta(\eta)$ and $\phi(\eta)$ in the boundary layer. The fourth order Runge-Kutta integration method is used to solve this system of simultaneous equations once all beginning conditions have been met.The value of $\eta_\infty$is selected to 10 depending on the physical factors controlling the flow in order to prevent numerical oscillation. Consequently, the third-order linked boundary value issue in$f(\eta)$, second-order in $\theta(\eta)$ and $\phi(\eta)$ has been simplified to the system of seven first-order simultaneous equations for seven unknowns below.

$$\left.\begin{aligned} & f' = p \Rightarrow f'' = p' = q \Rightarrow f''' = p'' = q' \Rightarrow q' = \frac{Mp + Kp - fq + 2p^2}{\{(1-n) - n\lambda q\}} \\ & \theta' = r \Rightarrow \theta'' = r' \text{ then } r' = \frac{-(\Pr) fr + \Pr p\theta - (\Pr)(Nb) rz - (\Pr)(Nt) r^2}{\left(1 + \frac{4R}{3}\right)} \\ & \& \\ & \phi' = z \Rightarrow \phi'' = z' \text{ then } z' = \frac{-(Sc)(Nb) fz - (Nt) r' - (\beta)(Nb)\phi}{Nb} \end{aligned}\right\} \quad (22)$$

and the associated boundary constraints evolved into

$$\left.\begin{aligned} & p(0) = 1,\ f(0) = S,\ \theta(0) = 1 + \delta r(0),\ \phi(0) = 1 + \Delta z(0), \\ & \&\ p(\infty) \to 0,\ \theta(\infty) \to 0,\ \phi(\infty) \to 0 \end{aligned}\right\} \quad (23)$$

First, a primary value problem(IVP) is created from the boundary value problem.Whichreceives more investigation .The shooting approach is then used to accurately predict the missing beginning value for different element combinations. Until the beginning value problem is resolved, these steps are repeated.In this case, calculations are made using the step size h = 0.1. Furthermore, an error tolerance of 10-6 is being employed. The data is displayed as tables and graphs, thoroughly examining and addressing the key aspects of the issues at hand.

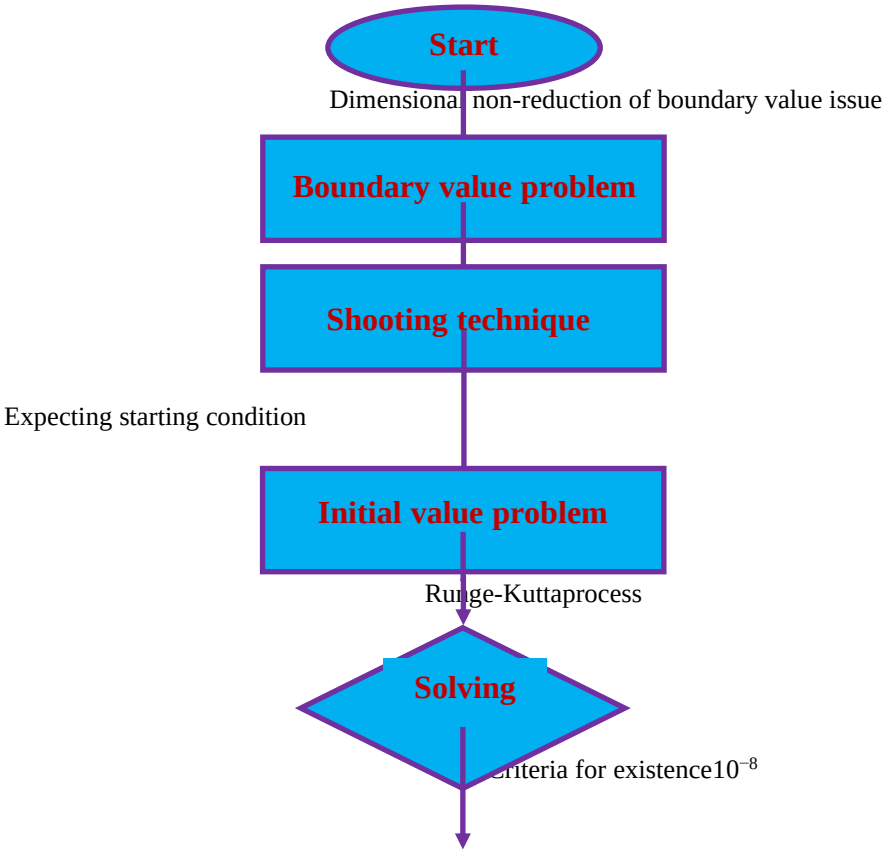

Fig. 2: A flow chart illustrating the numerical process

4. Validation of Program Code:

For validation of program code, the authors have compared the exixstingresults ofthe coefficient of skin friction with the results that have been released ofAkbar et al. [26], Malik et al. [27], Hussain et al. [28] and Waqas et al. [29] in absence of λ(Williamson fluid parameter), n(parameter of Power law index), K(Permeability parameter), ϑ (Stretching sheet parameter), R(Parameter of Thermal radiation), β(Chemical reaction's parameter), δ(parameter of Thermal slip) and Δ(Concentration slip parameter) for variousvalues of M(parameter of Magnetic field) in table-1.This table's comparison explains that the results are in extremely good agreement with the published results.

Table 1: Comparing the skin-friction's coefficient results with previous findings in the lack of λ, n, K, R, β, ϑ, δ and Δ for various values of M

M	Akbar et al. [26]	Malik et al. [27]	Hussain et al. [28]	Waqas et al. [29]	Present results
1	– 1.41421	– 1.41419	– 1.4137	– 1.4142	– 1.4098852364
5	– 2.449449	– 2.44945	– 2.4495	– 2.4495	– 2.4367859292
10	– 3.31663	– 3.31657	– 3.3166	– 3.3166	– 3.3067892987
100	– 10.0498	– 10.04981	– 10.0500	– 10.0500	– 10.0496780933
500	– 22.38303	– 22.38294	– 22.3835	– 22.3835	– 22.3767678208
1000	– 31.63859	– 31.63851	– 31.6391	– 31.6391	– 31.6257907370

5. Results and Discussion:

Currently being studied are the impacts of the field of magnetic, thermophoresis, Brownian motion, and multiple slips (thermal and concentration slips) on the boundaries of the layer's concentration and temperature. The R-K technique and the shooting methodology were used to finish the work-around for the governing difficulties, and the results are visibly shown to show how the problem behaves. The contribution of several physical components is examined in this research, adding the Magnetic field factor($M \in [0.1, 0.8]$), parameter of the Permeability($K \in [0.3, 1.0]$), Williamson element ($\lambda \in [0.2, 1.0]$), Parameter of Power-law index ($n \in [0.2, 1.0]$), Suction/Injection parameter ($S \in [-0.8, 0.8]$),Stretching sheet factor ($\vartheta \in [0.2, 1.2]$), Prandtl number ($\mathrm{Pr} \in [0.71, 7.0]$), factor of Thermal radiation ($R \in [0.5, 1.2]$), Brownian motion element ($Nb \in [0.3, 1.0]$), Thermophoresis factor ($Nt \in [0.3, 1.0]$), Schmidt number ($Sc \in [0.22, 0.78]$), Chemical reaction parameter ($\beta \in [0.3, 1.0]$), Thermal slip parameter ($\delta \in [0.3, 1.0]$), Concentration slip parameter ($\Delta \in [0.1, 1.0]$) on temperature distribution, concentration distribution, and velocity distribution are examined. The action of the significant analysis is done on components namely the Sherwood number, Nusselt number, and skin-friction coefficient..We investigated a wide range of statistical techniques.for example $M = 0.1$, $K = 0.3$, $\lambda = 0.2$, $n = 0.2$, $S = -0.8$ (Suction), $S = 0.8$ (Injection), $\vartheta = 0.2$, $\mathrm{Pr} = 0.71$, $R = 0.5$, $Nb = 0.3$, $Nt = 0.3$, $Sc = 0.22$, $\beta = 0.3$, $\delta = 0.1$ and $\Delta = 0.1$. Throughout the essay, the values of these variables remain constant unless otherwise noted, with the exception of pertinent tables and graphs to confirm parameter variations.

- Magnetic field parameter ($M \in [0.1, 0.8]$) variations on velocity profiles are seen in Figure 3. A resistive force is also calledas the Lorentz force, which is created when M rises, is comparable to a drag force. The resistive forceslows the intensity of velocity, which slows its motion.
- Figure 4 depictsthe permeability factor ($K \in [0.3, 1.0]$) influence of on the profiles of the velocity. This graph shows that as the parameter of porosity K grows, so does the velocity profile. This is because the momentum barrier layer gets thinner and the porous layer gets noisier as K increases.
- The graphical implications of the Williamson element ($\lambda \in [0.2, 1.0]$) on the profile of velocity are shown and discussed in detail in Fig. 5. By incresingthe numerical values of λ in this picture, the fluid velocity is decreased in this image. The velocity profile is reduced as a result of the direct relationship between the Williamson parameter and relaxation time.
- The Power-law index factor impact ($n \in [0.2, 1.0]$) on the profilesof the velocity are discussed in Fig. 6. This graphic shows that when n values increase, the velocity profiles decrease.
- For our convenience, this graphic Fig. 7 illustrates the effect of the suction/injection parameter ($S \in [-0.8, 0.8]$) on the dimensionless velocity. According to Fig. 7, S has a significant impact on thickness of the boundary layer. As S increases, the flow seems to be significantly impeded. There's less momentum and less velocity as a result of suction/injection. By moving momentum, the suction/injection lowers the thickness of this boundary layer, reducing its thickness.
- Fig. 8, for variate values of Stretching sheet parameter ($\vartheta \in [0.2, 1.2]$)the velocity profiles depicts. By definition, Stretching sheet parameter ϑ indicates the proportion of the y-to x-direction stretching rates. The value of the stretching rate ratio parameter not only improves the velocity profiles in the x-direction but also increases the velocity in the y-direction, as this picture illustrates.
- Fig. 9illustrates how the the temperature field affects by Prandtl number ($\mathrm{Pr} \in [0.71, 7.0]$).It has shown that when the Prandtl number Pr increases, the temperature field and thermal layer density decrease. Physically, reduced temperature is caused by thermal diffusivity since Prandtl number Pr is a crucial component of thermal diffusivity. Heavy thermal diffusivity is produced by larger Prandtl numbers, and this correlates to a lower temperature field and a thinner thermal layer.
- Fig.10 displays the variations in temperature profiles brought about by an increase in the values of ($R \in [0.5, 1.2]$). In the presence of R, the nanofluid's conduction effect intensifies, leading to the observation that the fluid temperature rises as R increases. Increased surface heat flow, which is implied by larger values of R, raises the boundary layer's internal temperature area.
- Fig. 11displays the temperature field's fluctuation for various Brownian motion parameter values($Nb \in [0.3, 1.0]$). This figure clearly shows that a rise in the Brownian motion parameter Nb resulted in an amplification of the thermal layer thickness and the associated temperature field.

- From Fig. 12,it is explained unequivocally that a higher Brownian motion parameter results in a weaker concentration field. ($Nb \in [0.3, 1.0]$).
- Fig. 13is illustrated to show how the thermophoresis factor ($Nt \in [0.3, 1.0]$), the field of temperature. Elevated the thermophoresis parameter Ntvalues signify an elevated temperature domain and an increased thermal layer.This theory is supported by the fact that a greater Nt results a greater temperature field and a thicker thermal layer are created by a stronger thermophoretic force that enables deeper mobility of nanoparticles in the fluid further from the surface.
- Fig. 14higher parameter for thermophoresis ($Nt \in [0.3, 1.0]$) shows that the,cause the concentration field to get stronger.
- Fig. 15 shows how the thermal slip parameter affects it. ($\delta \in [0.1, 0.8]$)on the dimensionless profiles of temperature. It is clear that when δ increases, temperature profiles decrease. Even in the case of a negligible transfer of heat from the sheet to the fluid, the thermal boundary layer thickness decreases with increasing value of the thermal slip parameter.
- The impact of increasing the reaction rate parameter ($\beta \in [0.3, 1.0]$) Fig. 16 shows the profiles of species concentrations to produce chemical reactions.This graph demonstrates that there is a noticeable effect when the chemical reaction rate parameter β is raised, on the solutal boundary layer concentration distribution when the chemical reaction rate parameter β is raised, on the solutal boundary layer concentration distribution.This graphic clearly illustrates how the species concentration at the boundary layer's beginning decreases for all reaction rate parameter values, eventually reaching zero as the boundary layer's smallest value. Notably, species concentration in the boundary layer falls as the chemical reaction rate parameter value rises; this is because the solutal border layer shrinks with β.
- The influence of concentration slip component ($\Delta \in [0.1, 1.0]$)) onprofiles of concentration is discussed in Fig. 17. As the increasesof concentration slip parameter (Δ), it can be seen from this figure that the concentration profiles are decreasing.
- The concentration profiles (ϕ)variation of for the assessment of Schmidt constant number ($Sc \in [0.22, 0.78]$) can be evaluated from Fig. 18. We notice that the concentration of nanoparticles is declining for growing values of Schmidt number (Sc). The boundary layer thicknesses of concentration and momentum is used to calculate the Schmidt number. Mass diffusion exceeds momentum when Sc is small. Therefore, in comparison to the momentum boundary layer, the concentration boundary layer is thicker.
- Table-2provides the Skin-Friction Coefficient values in numerical form for varying engineering parameter values such as, Parameter of Magneticfield ($M \in [0.1, 0.8]$), Permeability parameter ($K \in [0.3, 1.0]$), Williamson component ($\lambda \in [0.2, 1.0]$), parameterof Power-law index ($n \in [0.2, 1.0]$), Suction/Injection parameter ($S \in [-0.8, 0.8]$), parameter of Stretching sheet ($\vartheta \in [0.2, 1.2]$), Prandtl number ($\Pr \in [0.71, 7.0]$), parameter of Thermal radiation ($R \in [0.5, 1.2]$), Brownian motion parameter ($Nb \in [0.3, 1.0]$), parameter of Thermophoresis ($Nt \in [0.3, 1.0]$), Schmidt number ($Sc \in [0.22, 0.78]$), Chemical reaction parameter ($\beta \in [0.3, 1.0]$), Thermal slip parameter ($\delta \in [0.3, 1.0]$), Concentration slip parameter ($\Delta \in [0.1, 1.0]$).This table shows that when the values ofStretching sheet parameter ($\vartheta \in [0.2, 1.2]$) increase, the Skin-friction coefficient increases., Thermal radiation parameter ($R \in [0.5, 1.2]$), Brownian motion parameter ($Nb \in [0.3, 1.0]$), Thermophoresis parameter ($Nt \in [0.3, 1.0]$), When the magnetic field parameter ($M \in [0.1, 0.8]$) values increase, it decreases, parameter of Permeability ($K \in [0.3, 1.0]$), Williamson parameter ($\lambda \in [0.2, 1.0]$), Power-law index parameter($n \in [0.2, 1.0]$), Suction/Injection parameter ($S \in [-0.8, 0.8]$), Prandtl number ($\Pr \in [0.71, 7.0]$), Schmidt number ($Sc \in [0.22, 0.78]$), Chemical reaction parameter ($\beta \in [0.3, 1.0]$), Thermal slip parameter ($\delta \in [0.3, 1.0]$), Concentration slip parameter ($\Delta \in [0.1, 1.0]$).
- The Nusselt numbernumerical valuesor heat transfer coefficient rate are shows in table-3 for different values of Prandtl number ($\Pr \in [0.71, 7.0]$), Thermal radiation's parameter ($R \in [0.5, 1.2]$), Brownian motion parameter ($Nb \in [0.3, 1.0]$), Thermophoresis parameter ($Nt \in [0.3, 1.0]$) and Thermal slip parameter ($\delta \in [0.1, 0.8]$). The heat transfer coefficient rate is seen to increase with increasing values

of in this table.Thermal radiation parameter($R \in [0.5, 1.2]$), Brownian motion parameter ($Nb \in [0.3, 1.0]$), Thermophoresis parameter($Nt \in [0.3, 1.0]$), as it is getting smaller as the values rise of Prandtl number ($\Pr \in [0.71, 7.0]$), and Thermal slip parameter ($\delta \in [0.1, 0.8]$).

- The joint effects of ofBrownian motion's parameter ($Nb \in [0.3, 1.0]$), parameter of Thermophoresi($Nt \in [0.3, 1.0]$), Schmidt number ($Sc \in [0.22, 0.78]$), Chemical reaction parameter ($\beta \in [0.3, 1.0]$), Concentration slip parameter ($\Delta \in [0.1, 1.0]$)on rate of coefficient of mass transfer are discussed in Table-4. This table shows that the rate of mass transfer coefficient increases as the thermophoresis parameter ($Nt \in [0.3, 1.0]$), while it decreases as the parameter of Brownian motion ($Nb \in [0.3, 1.0]$)and decreasing with rising values of parameter of Brownian motion, Schmidt number ($Sc \in [0.22, 0.78]$), Chemical reaction parameter ($\beta \in [0.3, 1.0]$), Concentration slip parameter ($\Delta \in [0.1, 1.0]$).

Table-2: values of theparameterof Skin-friction in Numerical x for variousoutcomes of M,K,λ,n,S,ϑ,Pr, R, Nb, Nt, δ, Sc, β and Δ

M	K	λ	n	S	ϑ	Pr	R	Nb	Nt	δ	Sc	β	Δ	Cf
0.1	0.3	0.2	0.2	– 0.8	0.2	0.71	0.5	0.3	0.3	0.1	0.22	0.3	0.1	– 1.765367986096
0.3														– 1.806787908711
0.5														– 1.824536946487
	0.6													– 1.796576518076
	0.9													– 1.811376824510
		0.5												– 1.791690347035
		0.8												– 1.818761601303
			0.5											– 1.789567360743
			0.7											– 1.808678410466
				– 0.5										– 1.786786980137
				0.5										– 1.809852091739
				0.8										– 1.819454651964
					0.5									– 1.746786037093
					0.8									– 1.729561734601
						1.00								– 1.795138738743
						3.00								– 1.810857189733
							0.8							– 1.780847897116
							1.0							– 1.809556871804
								0.6						– 1.745670173403
								0.8						– 1.725566198699
									0.5					– 1.739661837406
									0.8					– 1.716782903981
										0.4				– 1.779861993467
										0.6				– 1.796780937498
											0.30			– 1.788167275802
											0.78			– 1.802254567348
												0.6		– 1.770867986798
												0.9		– 1.782376348760
													0.4	– 1.776268679819
													0.8	– 1.789857198373

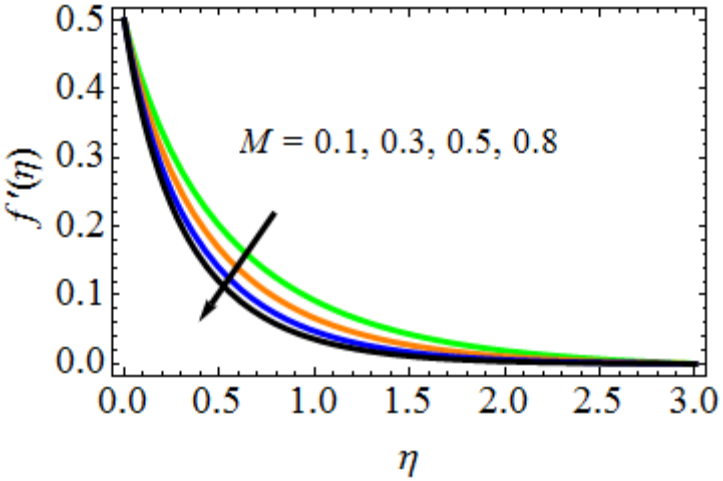

Fig 3: *M*influence onprofiles of velocity

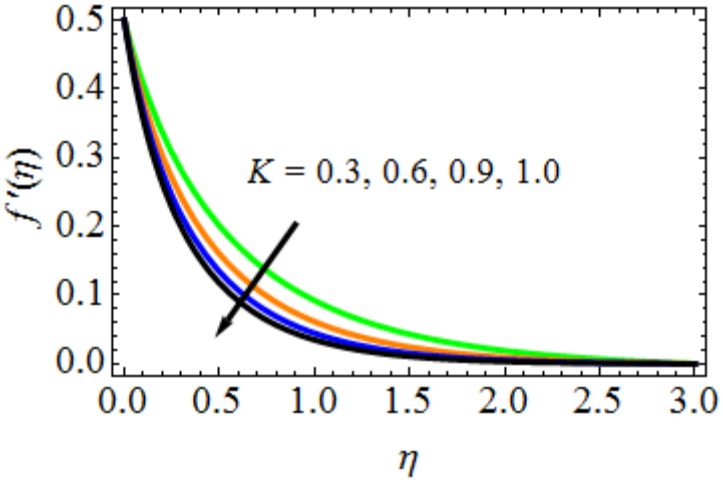

Fig 4: *K* effect on profiles of velocity

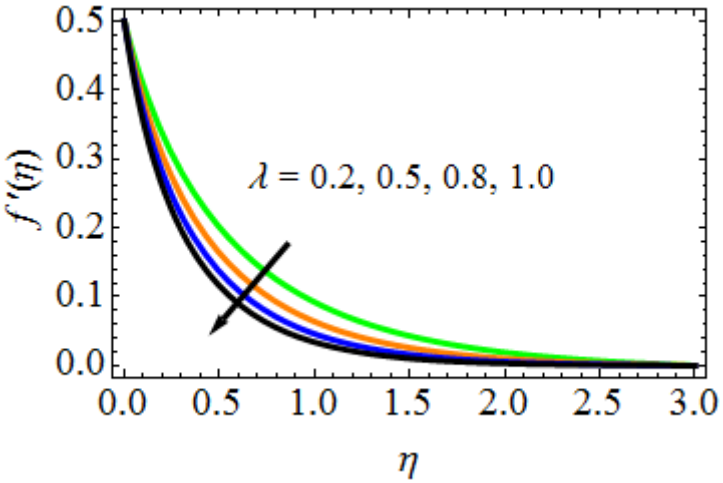

Fig 5: λ impact on profiles of velocity

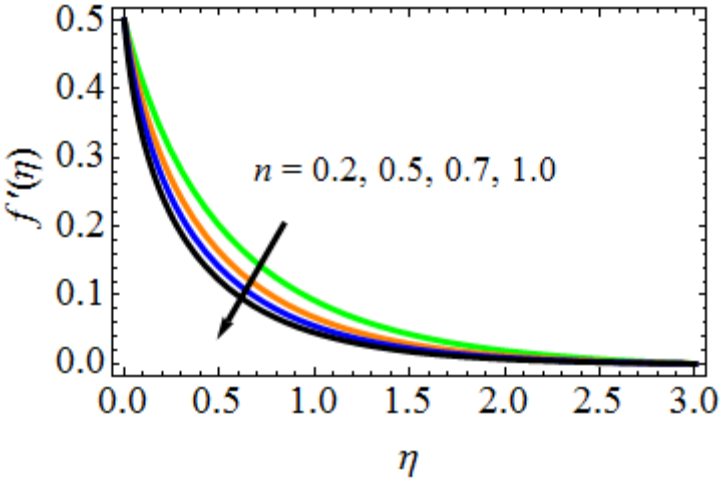

Fig 6: *n* impact on profiles of velocity

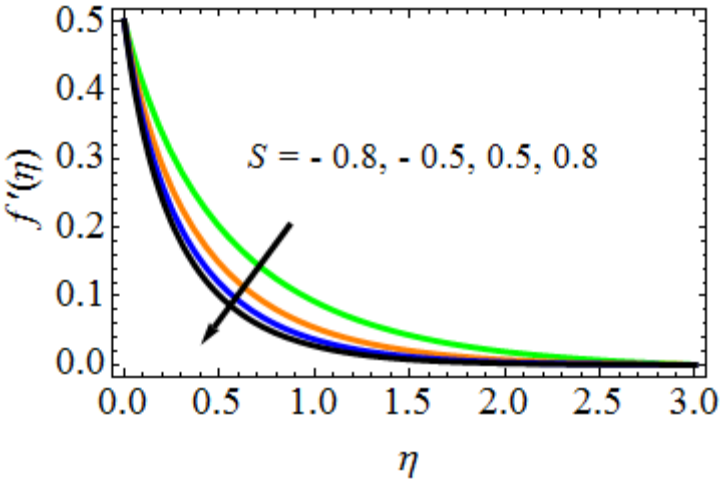

Fig. 7: *S* effect on profiles of velocity

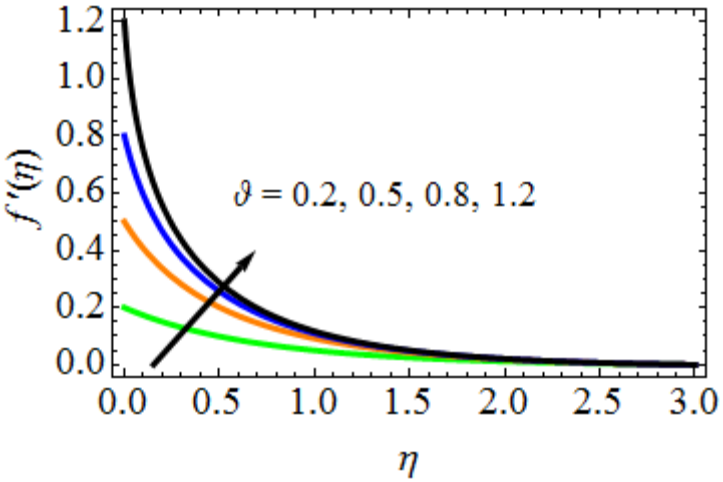

Fig. 8: ϑ influence on profiles of velocity

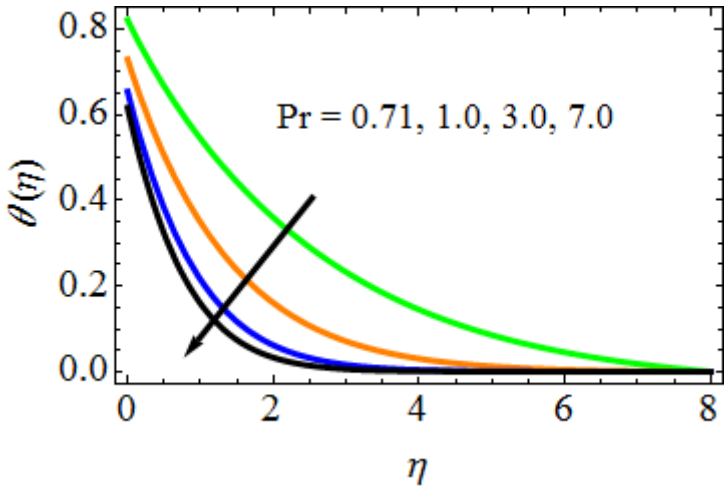

Fig. 9: Preffect on profiles temperature

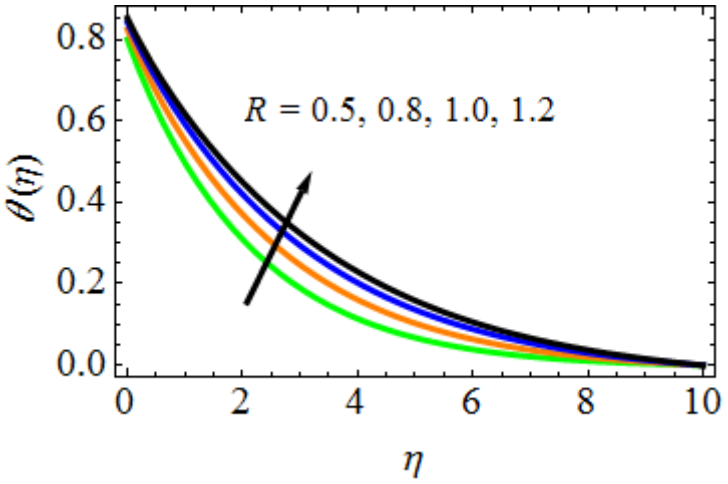

Fig. 10: *R* influence on temperature profiles

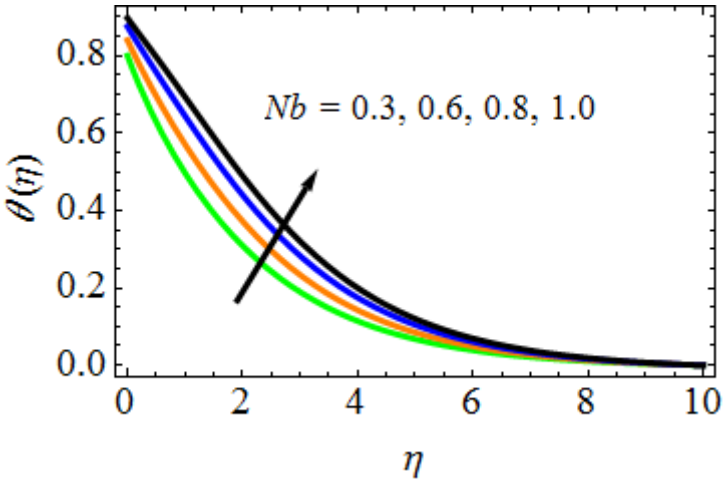

Fig. 11: *Nb* impactprofiles on temperature

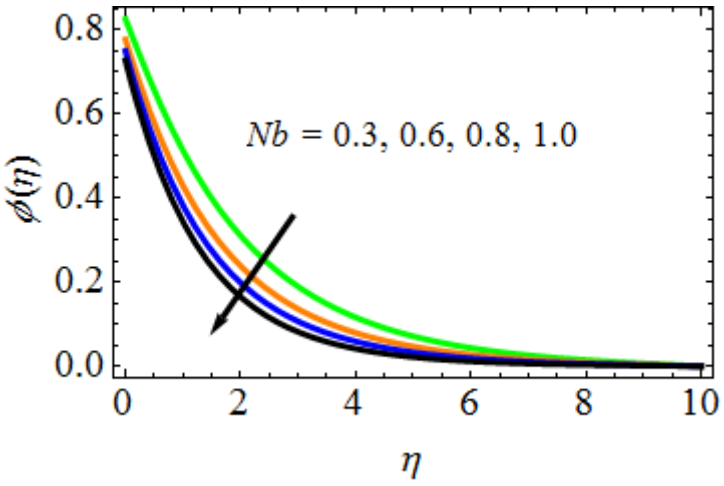

Fig. 12: *Nb* effect onprofiles of concentration

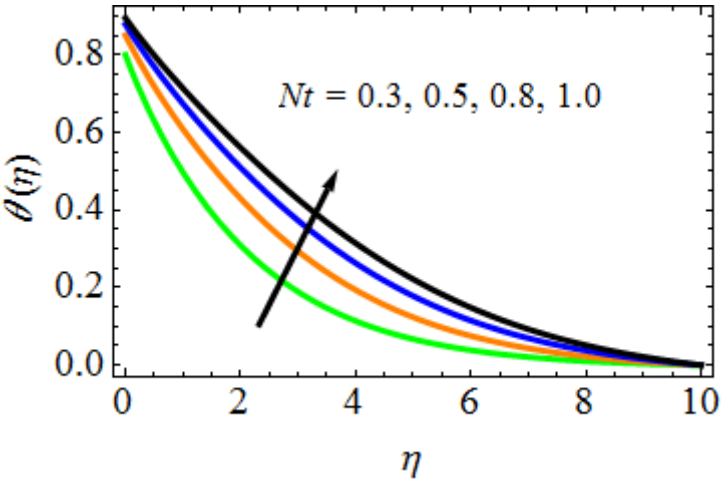

Fig. 13: *Nt*effect on profiles of concentration

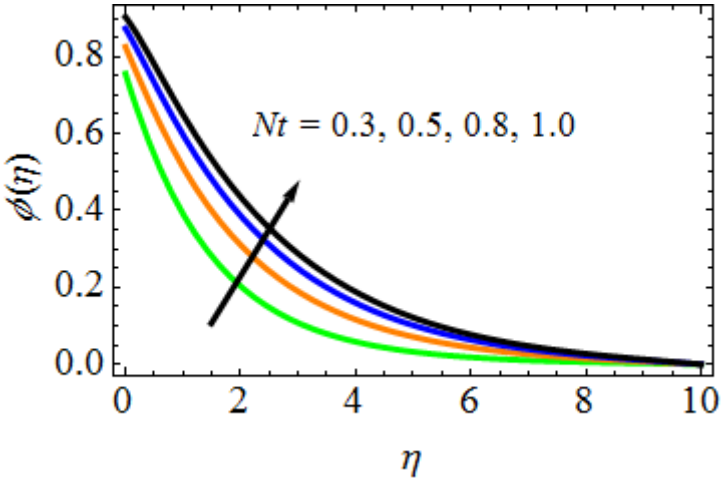

Fig. 14: *Nt*effect on profiles concentration

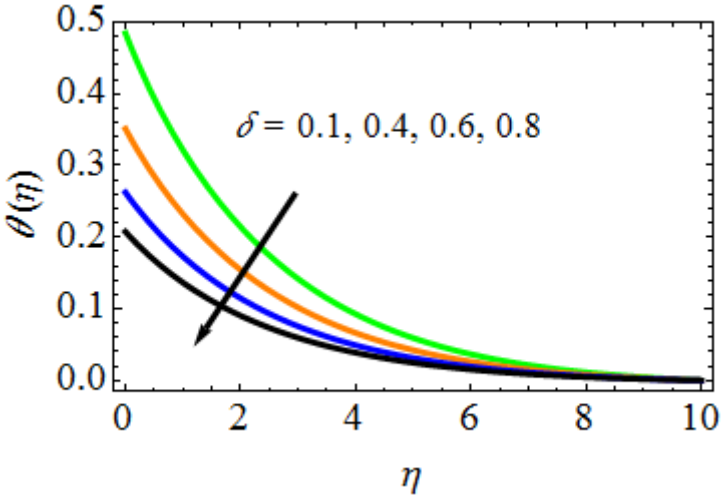

Fig. 15: δ effect on profiles of concentration

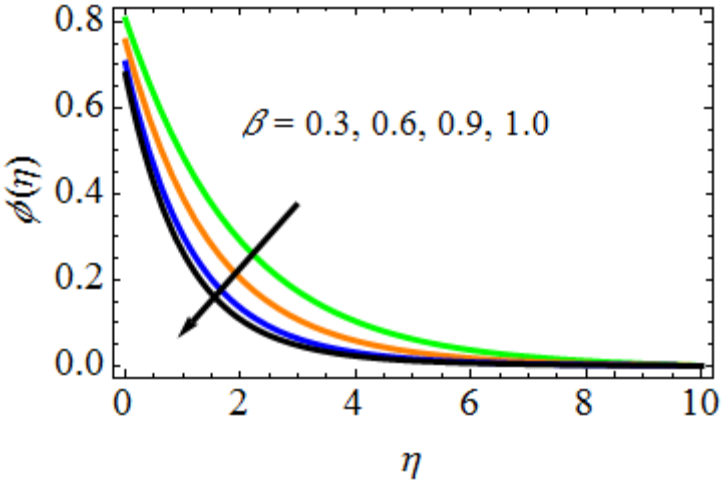

Fig. 16: β effect on profiles of concentration

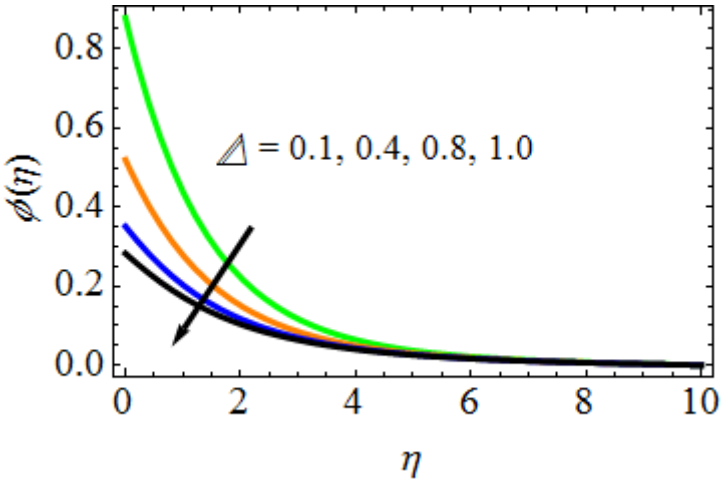

Fig. 17: Δ profiles

Table 3: The heat transfer coefficient's rate in numerical values for various values of Pr,*R*,*Nb*,*Nt*, and δ

Pr	*R*	*Nb*	*Nt*	Δ	*Nu*
0.71	0.5	0.3	0.3	0.1	2.678279379394
1.00					2.637813896933
3.00					2.609831393915
	0.8				2.702857901437
	1.0				2.727663476762
		0.6			2.692567875847
		0.8			2.711567438718
			0.5		2.705678791853
			0.8		2.721657687329
				0.4	2.646788238082
				0.6	2.627883760391

Table 4: Mass transfer coefficient rate values in Numerical of for various values of *Sc*,*Nb*,*Nt*,β, and Δ

Nb	*Nt*	*Sc*	β	Δ	*Sh*
0.3	0.3	0.22	0.3	0.1	2.879676380360
0.6					2.849867170163
0.8					2.826570760436
	0.5				2.901567283469
	0.8				2.926787368795
		0.30			2.847777606343
		0.78			2.807983763012
			0.6		2.859867360398
			0.9		2.834578687468
				0.4	2.841756076034
				0.8	2.819658763407

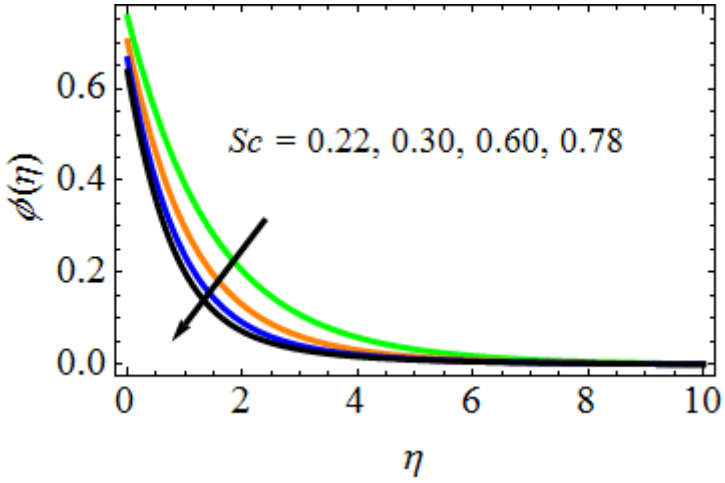

Fig. 18: *Sc* influence on concentration profiles

6. Conclusions:

During this work, the authors have explored a permeable stretched sheet submerged in a porous fluid, causing various slip effects, heat radiation, thermophoresis, chemical reaction, and MHD. The result is a stable two-dimensional, viscous, incompressible, and electrically conductive WNF.To evaluate the controlling flow model, the shooting technique was combined with the RK approach.. Tables and diagrams were used to illustrate the physical characteristics at play. By comparing the results to past data obtained under various assumptions, the validity of the findings was investigated, and very similar results were obtained. From the combined quantitative and graphical data, some important conclusions were reached, including: The fluid parameters' function as a reduction function for the magnetic field's parameter($M \in [0.1, 0.8]$) in the velocity distribution was discussed below.Parameter of Permeability ($K \in [0.3, 1.0]$), Williamson parameter ($\lambda \in [0.2, 1.0]$), Power-law index parameter ($n \in [0.2, 1.0]$), Suction/Injection parameter ($S \in [-0.8, 0.8]$), and Stretching sheet parameter ($\vartheta \in [0.2, 1.2]$). As can be seen below, the temperature field's numerous parameters had all produced increasing values.:Thermal radiation's parameter ($R \in [0.5, 1.2]$), Brownian motion parameter ($Nb \in [0.3, 1.0]$), Thermophoresis parameter ($Nt \in [0.3, 1.0]$). In the reverse manner a temperature distribution that operates, was analyzed when the values forPrandtl number ($\Pr \in [0.71, 7.0]$) andparameter of Thermal slip ($\delta \in [0.3, 1.0]$) are decreased. The concentration profiles show higher values for high levels of parameter of Thermophoresis ($Nt \in [0.3, 1.0]$). With increasing Brownian motion parameter ($Nb \in [0.3, 1.0]$), Schmidt number ($Sc \in [0.22, 0.78]$), Chemical reaction parameter ($\beta \in [0.3, 1.0]$), and Concentration slip parameter ($\Delta \in [0.1, 1.0]$), the concentration field exhibits the opposite behavior.
In the future, the authors havewish to build on this work by examining mass and heat fluxes to regulate the cooling process with a non-Newtonian nanofluid.

References

[1] R.V. Williamson, The flow of pseudoplastic materials, Ind. Eng. Chem., 21 (1929), pp. 1108-1111, 10.1021/ie50239a035.

[2] K.A. Kumar, J.V.R. Reddy, V. Sugunamma, N. Sandeep, Simultaneous solutions for MHD flow of Williamson fluid over a curved sheet with non-uniform heat source/sink, Heat Tran. Res., 50 (2019), pp. 581-603.

[3] K. Ahmed, W.A. Khan, T. Akbar, G. Rasool, S.O. Alharbi, I. Khan, Numerical investigation of mixed convective Williamson fluid flow over an exponentially stretching permeable curved surface, Fluid, 6 (7) (2021), p. 260.

[4] L.A. Lund, Z. Omar, I. Khan, Analysis of dual solution for MHD flow of Williamson fluid with slippage, Heliyon, 5 (2019), 10.1016/j.heliyon.2019.e01345.

[5] K.A. Kumar, J.V. Ramana Reddy, V. Sugunamma, N. Sandeep, MHD flow of chemically reacting Williamson fluid over a curved/flat surface with variable heat source/sink, Int. J. Fluid Mech. Res., 46 (2019), pp. 407-425.

[6] A. M. Megahed, Steady flow of MHD Williamson fluid due to a continuously moving surface with viscous dissipation and slip velocity, Int. J. Mod. Phys. C, 31 (2020), pp. 1-12.

[7] B. J. Gireesha, S. Sindhu, G. Sowmya, A. Felicita, Magnetohydrodynamic flow of Williamson fluid in a microchannel for both horizontal and inclined loci with wall shear properties, Heat Transf., (2020), pp. 1-15,

[8] Bhatti M.M., Arain M.B., Zeeshan A., Ellahi R., Doranehgard M.H., Swimming of gyrotactic microorganism in MHD Williamson nanofluid flow between rotating circular plates embedded in porous medium: Application of thermal energy storage, J Energy Storage, 45 (2022), Article 103511.

[9] Dawar A., Shah Z., Islam S., Mathematical modeling and study of MHD flow of Williamson nanofluid over a nonlinear stretching plate with activation energy, Heat Transfer, 50 (3) (2021), pp. 2558-2570.

[10] Li Y.X., Alshbool M.H., Lv Y.P., Khan I., Khan M.R., Issakhov A., Heat and mass transfer in MHD Williamson nanofluid flow over an exponentially porous stretching surface, Case Stud Therm Eng, 26 (2021), Article 100975

[11] V.S. Patil, P.P. Humane, A.B. Patil, MHD Williamson nanofluid flow past a permeable stretching sheet with thermal radiation and chemical reaction, Int. J. Modell. Simulat. (2022), pp. 1-15.

[12] A.U. Awan, S.A.A. Shah, B. Ali, Bio-convection effects on Williamson nanofluid flow with exponential heat source and motile microorganism over a stretching sheet, Chinese J. Phys., 77 (2022), pp. 2795-2810.

[13] K. Ahmed, W.A. Khan, T. Akbar, G. Rasool, S.O. Alharbi, I. Khan, Numerical investigation of mixed convective Williamson fluid flow over an exponentially stretching permeable curved surface, Fluids, 6 (7) (2021), p. 260.

[14] U. Nazir, M.A. Sadiq, M. Nawaz, Non-Fourier thermal and mass transport in hybridnano-Williamson fluid under chemical reaction in Forchheimer porous medium, Int. Commun. Heat Mass Transfer, 127 (2021), p. 105536.

[15] Yahaya Shagaiya Daniel, Zainal Abdul Aziz, Zuhaila Ismail, Arifah Bahar, Faisal Salah, Stratified electromagnetohydrodynamic flow of nanofluid supporting convective role, Korean J. Chem. Eng., 36 (7) (2019), pp. 1021-1032.

[16] Yahaya Shagaiya Daniel, Zainal Abdul Aziz, Zuhaila Ismail, Faisal Salah, Effects of thermal radiation, viscous and Joule heating on electrical MHD nanofluid with double stratification, Chin. J. Phys., 55 (3) (2017), pp. 630-651.

[17] Yahaya Shagaiya Daniel, Zainal Abdul Aziz, Zuhaila Ismail, Faisal Salah, Double stratification effects on unsteady electrical MHD mixed convection flow of nanofluid with viscous dissipation and Joule heating, J. Appl. Res. Technol., 15 (5) (2017), pp. 464-476.

[18] F. Mabood, S.M. Ibrahim, G. Lorenzini, E. Lorenzini, Radiation effects on Williamson nanofluid flow over a heated surface with magnetohydrodynamics, Int. J. Heat Technol., 35 (1) (2017), pp. 196-204.

[19] Wubshet Ibrahim, Dachasa Gamachu, Nonlinear convection flow of Williamson nanofluid past radially stretching surface, AIP Adv., 9 (2019), Article 085026.

[20] Aamir Hamid, Mashood Khan Hashim, Matib Alghamdi, MHD Blasius flow of radiative Williamson nanofluid over a vertical plate, Int. J. Physics B, 33 (22) (2019), p. 1950245.

[21] H.M. Shawky, N.T.M. Eldabe, K.A. Kamel, Esmat A. Abd-Aziz, MHD flow with heat and mass transfer of Williamson nanofluid over stretching sheet through porous medium, Microsyst. Technol., 25 (2019), pp. 1155-1169.

[22] B.C. Prasannakumara, B.J. Gireesha, Rama S.R. Gorla, M.R. Krishnamurthy, Effects of chemical reaction and nonlinear thermal radiation on Williamson nanofluid slip flow over a stretching sheet embedded in a porous medium, J. Aerosp., Eng,29(5) (2016), 10.1061/(ASCE)AS.1943-5525.0000578.

[23] H.D. Hunegnaw, Unsteady Boundary layer flow of Williamson nanofluids over a heated permeable stretching sheet embedded in a porous medium in the presence of viscous dissipation, J. Nav. Archit. Mar. Eng., 18 (1) (2021), pp. 83-96.

[24] Kamran Ahmed, Tanvir Akbar, Numerical investigation of magnetohydrodynamics Williamson nanofluid flow over an exponentially stretching surface, Adv. Mech. Eng., 13 (5) (2021), pp. 1-12.

[25] A. Hamid Hashim, M. Khan, Heat and mass transport phenomena of nanoparticles on time-dependent flow of Williamson fluid towards heated surface, Neural Comput. & Appl., 32 (2019) (2020), pp. 3253-3263.

[26] N.S. Akbar, A. Ebaid, Z.H. Khan, Numerical analysis of magnetic field effects on Eyring-Powell fluid flow towards a stretching sheet, J. Magn. Magn. Mater. 382 (2015) 355-358.

[27] M.Y. Malik, T. Salahuddin, A. Hussain, S. Bilal, MHD flow of tangent hyperbolic fluid over a stretching cylinder: using Keller box method, J. Magn. Magn Mater. 395 (2015) 271-276.

[28] A. Hussain, M.Y. Malik, M. Awais, T. Salahuddin, S. Bilal, Computational and physical aspects of MHD Prandtl-Eyring fluid flow analysis over a stretching sheet, Neural Comput. Appl. 31 (2019) 425-433.

[29] H. Waqas, A. Kafait, T. Muhammad, U. Farooq, Numerical study for bio-convection flow of tangent hyperbolic nanofluid over a Riga plate with activation energy, Alexandria Eng. J. 61 (2022) 1803-1814.